Graphene Oxide Nanosheets Reshape Synaptic Function in Cultured Brain Networks

Graphene oxide nanosheets reshape synaptic function in cultured brain networks

Rossana Rauti[τ], Neus Lozano[§], Veronica León[‡], Denis Scaini[τ,#], Mattia Musto[ø], Ilaria Rago[#], Francesco P. Ulloa Severino[ø], Alessandra Fabbro[‖], Loredana Casalis[#], Ester Vázquez[‡], Kostas Kostarelos[§], Maurizio Prato[‖,&,ν] and Laura Ballerini[τ,ø]*

[τ]Life Science Department, University of Trieste, 34127 Trieste, Italy
[§]Nanomedicine Lab, School of Medicine and National Graphene Institute, Faculty of Medical & Human Sciences, University of Manchester, M13 9PL Manchester, United Kingdom
[‡]Departamento de Química Orgánica, Facultad de Ciencias y Tecnologías Químicas-IRICA Universidad de Castilla La-Mancha, 13071 Ciudad Real, Spain
[#]ELETTRA Synchrotron Light Source, 34149 Trieste, Italy
[ø]International School for Advanced Studies (SISSA), 34136 Trieste, Italy
[‖]Department of Chemical and Pharmaceutical Sciences, University of Trieste, 34127 Trieste, Italy
[&]CIC BiomaGUNE, Parque Tecnológico de San Sebastián, Paseo Miramón, 182, 20009 San Sebastián (Guipúzcoa), Spain
[ν]Basque Foundation for Science, Ikerbasque, Bilbao 48013, Spain

* Corresponding authors: Laura Ballerini International School for Advanced Studies (SISSA) via Bonomea 265 I-34136 Trieste laura.ballerini@sissa.it ; prato@units.it

Abstract

Graphene offers promising advantages for biomedical applications. However, adoption of graphene technology in biomedicine also poses important challenges in terms of understanding cell responses, cellular uptake or the intracellular fate of soluble graphene derivatives. In the biological microenvironment graphene nanosheets might interact with exposed cellular and subcellular structures resulting in unexpected regulation of sophisticated biological signaling. More broadly, biomedical devices based on the design of these 2D planar nanostructures for interventions in the central nervous system (CNS) requires an accurate understanding of their interactions with the neuronal milieu. Here, we describe the previously unreported ability of graphene oxide nanosheets to down-regulate neuronal signaling without affecting cell viability.

Keywords

Nanotechnology; graphene; patch-clamp; synaptic terminals; exocytosis; FMI-43; microvesicles.

Text

Graphene is a 2D plate-like material consisting of sp^2-hybridized carbon atoms organized in a hexagonal lattice and characterized by, among other properties, high electrical conductivity and mechanical flexibility[1-3]. In addition to the successful exploitation of graphene and graphene-based materials in an increasing number of industrial products, current applications of graphene hold the potential to revolutionize specific areas of medicine[2-6]. Biomedical developments in general, and in neurology in particular, are focusing on few-layer graphene sheets to manufacture novel bio-devices, including biosensors, interfaces, tissue scaffolds, drug delivery and gene therapy vector systems[4]. Successful design of multifunctional neuro-devices based on graphene will expose brain cells and neuronal circuits directly to this material by injection or implantation[4,7]. In this context, the exploration of the interactions between graphene nano- and micro-sheets with the sophisticated signaling machinery of nerve cells, with a particular focus on potential graphene flake interactions with the hydrophobic membrane domains, is of great importance[1,8,9]. Such interactions may favor graphene translocation, or adhesion to cell membranes[8,10], potentially interfering with exquisite membrane activities, such as the exocytic and endocytic trafficking systems, crucial to physiological synaptic transmission[8,11].

Here we explore for the first time by patch clamp and fluorescence imaging the ability of graphene (GR) and graphene oxide (GO) nanosheets to interfere with synaptic signaling once hippocampal cultured neurons are exposed for one week to a growth medium containing thin sheets of such materials at 1 or 10 μg/mL (concentrations reported not to induce cell death[12-14]).

We further investigated whether, in the absence of explicit cell toxicity, such materials affected the ability of astrocytes to release synaptic-like microvesicles[15] (MV) in pure glial cultures. Our results describe the potential of GO nanosheets to alter different modes of inter-neuronal communication systems in the CNS hinting at opportunities for novel neuromodulatory applications or highlighting subtle, but potentially unwanted, subcellular interactions.

Results and Discussion

To address the issue of prolonged exposure of a functional brain network to graphene sheets we used different materials. Graphene oxide sheets of large and small lateral dimensions (l-GO and s-GO, respectively) were synthesized using a modified-Hummers method (see Supporting Information). Following the reaction, the GO-gel like upper layer was extracted carefully by using warm water, resulting in the large GO (l-GO). Final concentrations ranged between 1 and 2mg/mL were obtained with a yield of ca. 10%. l-GO was freeze-dried, reconstituted in water for injection, sonicated for 5 mins and centrifuged at room temperature to generate the small GO (s-GO).The lateral dimension of GO sheets was controlled by drying and sonicating the l-GO to obtain the s-GO sheets, that were always at least one order of magnitude smaller, without introducing any significant changes among their surface properties (see Table S1).

The GO dispersions in aqueous media were homogenous, of brownish color and stable at room temperature for more than 6 months. The physicochemical characterization of the l-GO and s-GO dispersions is shown in Figure 1 (a-f), and in the Supporting Information Figure S1 and S2. Their structural properties (lateral dimension and thickness) were studied by optical microscopy, transmission electron microscopy (TEM) and atomic force microscopy (AFM). Optical properties were studied by UV-Vis and fluorescence spectroscopy. Raman spectroscopy and laser Doppler electrophoresis (measuring ζ–potential) were used to assess the surface properties of the GO materials. Their Raman spectrum showed D and G bands at 1319 cm^{-1} and 1596 cm^{-1}, respectively, characteristic of most poly-aromatic hydrocarbons. The D to G band intensity ratio (ID/IG) was calculated at 1.3, corresponding to the metric of disorder in the graphitic structure. The surface charge measured with a Zetasizer instrument showed an average ζ–potential of -50 mV, indicating flakes of high negative surface charge. To elucidate the degree of surface functionalization, thermo-gravimetric analysis (TGA) and X-ray photoelectron spectroscopy (XPS) survey spectra were performed to quantify the purity of the GO (> 99%) and the C:O ratio XPS high resolution C1s spectra were recorded to elucidate the contribution of individual functional groups such as carboxylic, carbonyl, epoxide and hydroxyl (Table S2b). All fittings shown were performed using the CasaXPS software and the different regions were assigned according to Nist XPs and lasurface databases. Deconvolution XPS spectra and assignment of

the functional groups indicated that hydroxyls were the least abundant species in the GO material produced (see also Supporting Information, Table S2a).

Aqueous dispersions of graphene (GR) flakes were prepared using ball-milling for the exfoliation of graphite through interaction with melamine, as previously described[16,17] (see Supporting Information). Due to the GR preparation process, graphene dispersions can contain traces of melamine. In order to determine the exact amount of these traces, final graphene dispersions (0.09 mg/mL) were evaluated by elemental analysis indicating 0.9 ppm of melamine. Experiments that involved incubation in neurons also included controls exposed to equal amounts of melamine alone (see Supporting Information). The physicochemical characterization of GR dispersions is shown in Figure S3. The lateral size, studied by TEM, was found to range between 500nm-3μm (Figure S3a-b). Optical properties were studied by UV-Vis absorption spectroscopy. Dispersions were diluted and their UV-Vis absorption spectra were recorded (Figure S3). The spectra are featureless in the Vis–NIR region, as expected. The absorbance at 660 nm, divided by cell length, is plotted against the concentration exhibiting Lambert-Beer behavior (Figure S3d). Raman spectroscopy revealed differences between the GO and GR. Graphene exhibits G and 2D modes around 1573 and 2700 cm-1, that satisfy Raman selection rules, while the D peak, around 1345 cm-1 requires a defect for its activation (Figure S3e). The D to G band intensity ratio was calculated at different locations, giving a significant low value (0.22) in comparison with GO. TGA was also used to quantify the functionalization degree of GR. The low weight loss observed in GR (7%) corroborated the low quantity of oxygen groups generated by the exfoliation process (Figure S3f).

We used hippocampal neurons isolated and cultured for 8-10 days *in vitro* (DIV). Primary neuronal cultures were incubated at 2 DIV in the presence of GR or s-GO (at 1 μg/mL and 10 μg/mL; see Supporting Information) maintained for 6 to 8 days and afterwards visually identified neurons were patch clamped under voltage clamp. Hippocampal neuron maturation and viability were assessed using single-cell recordings (see Supporting Information) to measure the cell passive membrane properties that are accepted indicators of neuronal health[18-20] that allowed comparison among the recorded cells. These parameters (membrane capacitance and input resistance) displayed similar values in all treatment conditions (summarized in Table 1).

Table 1. Neuronal passive membrane properties upon GR and s-GO exposure (1 μg/mL and 10 μg/mL respectively).

	Capacitance (pF)	Input Resistance (MΩ)
Control$_{n=24}$	59 ± 4	976 ± 138

$Melamine_{1\ n=28}$	46 ± 5	1036 ± 132
$s\text{-}GO_{1\ n=27}$	62 ± 8	876 ± 145
$GR_{1\ n=30}$	50 ± 5	1029 ± 161
$Control_{10\ n=20}$	57 ± 7	744 ± 82
$Melamine_{10\ n=25}$	72 ± 16	717 ± 106
$s\text{-}GO_{10\ n=18}$	67 ± 6	997 ± 156
$GR_{10\ n=25}$	59 ± 18	1223 ± 501

To investigate synapse formation and activity after *in vitro* growth of neurons, we monitored the occurrence of spontaneous postsynaptic currents (PSCs). The appearance of PSCs provided clear evidence of functional synapse formation and it is a widely accepted index of network efficacy[21,22].

Figure 1

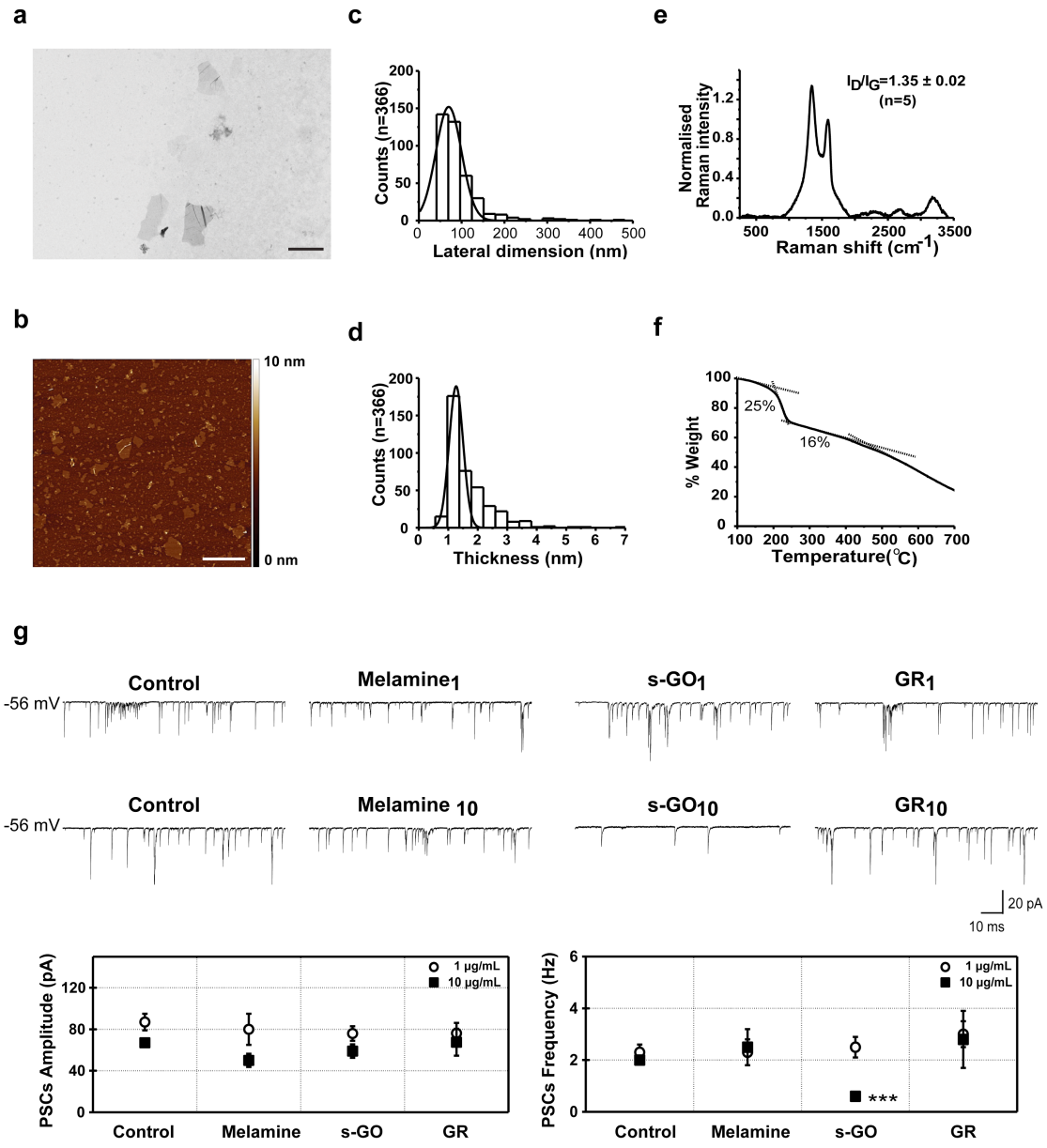

Figure 1. *Characterization of small graphene oxide (s-GO) of biological-grade; graphene oxide exposure at high concentration influences synaptic function.* In (a-f) physicochemical characterization of *s*-GO: (**a**) TEM micrograph (scale bar 1 μm). (**b**) AFM height image (scale bar 1 μm), (**c**) lateral dimension distribution and (**d**) thickness distribution analysis. (**e**) Normalized Raman spectrum. (**f**) TGA analysis. In (g) graphene oxide exposure at high concentration influences synaptic function. Spontaneous synaptic activity recorded from hippocampal cultures in control, melamine, s-GO and GR-treated cultures at 1 µg/mL (top traces) and 10 µg/mL (bottom traces) grown for 8 to 10 DIV. PSCs were detected at -56 mV holding potential. Bottom plots represent pooled data and summarize average PSCs amplitude and frequency: note the reduction in s-GO-treatment (10 µg/mL, final concentration) of PSCs frequency (*** = P < 0.001 Student's test, data are mean ± SEM).

Figure 1g, shows representative current tracings of the recorded electrical activity. In neurons exposed to low (1 μg/mL) s-GO and GR, spontaneous synaptic activity was not

affected. In fact, measured PSC amplitude and frequency in s-GO and GR (79 ± 7 pA and 2.5 ± 0.4 Hz n=27 and 77 ± 8 pA and 3 ± 0.5 Hz, n= 30, respectively) were comparable to the corresponding control and control-melamine values (87 ± 8 pA and 2.3 ± 0.3 Hz, control, n=24; 80 ± 15 pA and 2.3 ± 0.5 Hz melamine n= 28; plots in Figure 1 (g)). In all tests, cell parameters measured in melamine were comparable to those expressed by control neurons (Figure 1 (g) bottom plots), thus the impact on cells of such a contaminant at the estimated concentration is negligible.

When investigating the impact of higher graphene doses (10 μg/mL) we detected a significant difference ($P < 0.001$; Student's t-test) in PSC frequency when comparing control neurons (2.0 ± 0.1 Hz control, n= 20) with s-GO treated ones (0.6 ± 0.1 Hz, n= 18), while in melamine and GR, PSC frequency values remained unchanged (2.5 ± 0.7 Hz melamine, n= 25 and 2.8 ± 1.1 Hz GR; n= 25). In all treatments studied, the amplitude values of the PSCs were never affected (data are summarized in Figure 1 (g) plots). We further tested synaptic responses when neurons were treated (1 and 10μg/mL) with a commercially available GO provided by an industrial partner (A-GO; Supporting Information and Figures S4). Similar reduction in PSC frequency (Figure S5) was detected that validated the observation that GO nanosheets, differently to GR flakes, specifically interfered with synapses in cultured neurons, regardless of the starting material.

Figure 2

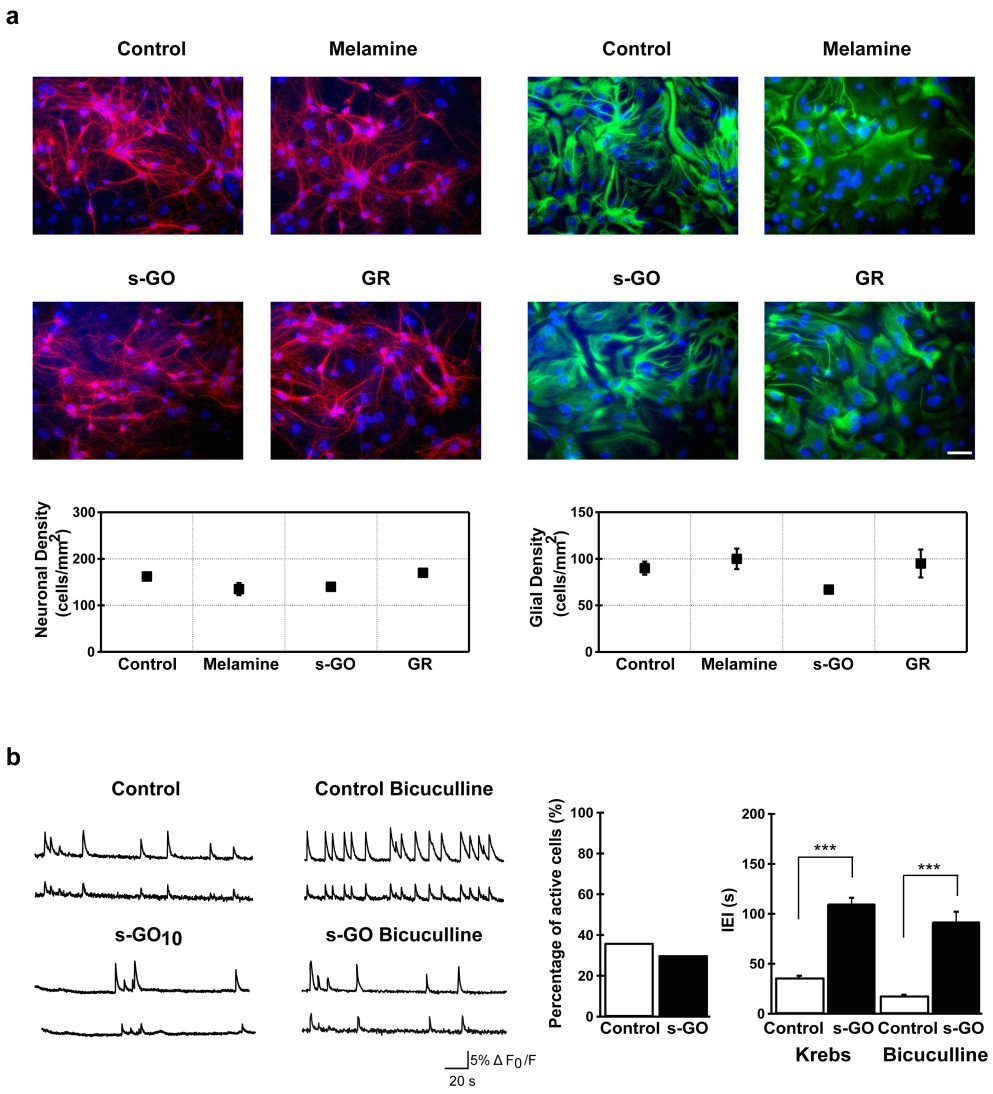

Figure 2. *s-GO exposure at high concentration impaired network activity without changing network size.* In (a) immunofluorescence images are shown to visualize neurons and glial cells in the 4 different conditions (anti β-tubulin III, in red, left panels; anti-GFAP, in green, right panels, in all nuclei are visualized by DAPI in blue) (samples are for the 10 μg/mL protocol; scale bar 50 μm). The plots summarize neuronal (left) and glial (right) densities in all conditions. In (b) repetitive Ca^{2+}-oscillations spontaneously (left panel) or bicuculline-induced (right panel) recorded in hippocampal cultures at 8 to 10 DIV (from each field sample recordings of 2 cells were selected). Histograms summarize the percentage of spontaneous active cells (middle) and the average values of the inter-event-interval (IEI; right) in standard saline (Krebs) and in the presence of bicuculline (*** = $P < 0.001$ Student's-t-test, data are mean ± SEM).

The impact of 10 μg/mL s-GO on synaptic activity was not related to a decreased number of surviving neurons in the presence of s-GO. In fact, we determined the cellular composition of control and s-GO treated hippocampal cultures using immunofluorescence markers[23] for astrocytes (GFAP) and neurons (β-tubulin III). We observed both β-tubulin III and GFAP immunoreactive cells in all growing conditions (Figure 2 (a)) and both cell groups were represented in a comparable proportion in all treatment groups (quantified by measuring the cell

density in Figure 2 (a), (n=13 visual field per condition, 3 different culture series). Thus s-GO at higher concentrations specifically altered synapse formation and/or function without affecting cell survival or the global network size.

To gain more insight into such processes we further investigated s-GO-treated (10 μg/mL) cultures. We specifically addressed the distribution of neuronal excitation by measuring the activity of small clusters of neurons with fluorescence calcium imaging[23-25]. On average 7±2 fluorescent neurons (n=26 fields), stained with the membrane permeable Ca^{2+} dye Fura-2-AM (see Supporting Information), were simultaneously visualized in the recorded field (120 x 160 μm^2). We compared and characterized the cell ability to generate repetitive Ca^{2+} oscillations[23-25]. In control conditions all recorded fields (n=8) displayed active cells, while in s-GO treated cells 56% (n=10 out of 18) of the recorded fields did not display detectable cell activity. However, in the remaining s-GO fields (n=8), we found an amount of neurons that were spontaneously generating repetitive Ca^{2+} oscillations comparable to that measured in controls (Figure 2 (b), 36% in control, 20 out of 56 neurons, n=8 active fields and 30% in s-GO-treated, 18 out of 60 neurons, n=8 active fields).

Figure 2 (b) traces represent fluorescence recordings from active fields in control and s-GO-treated cultures (2 sampled cells in each field). Episodes usually comprised spontaneous bursts of activity, fully blocked by tetrodotoxin (TTX,, a blocker of voltage-gated, fast Na^+ channels) applications (1 μM; n= 8 fields, control and s-GO-treated; not shown). Control Ca^{2+} oscillations displayed an inter-event interval (IEI) of 36 ± 2 s (n=20 cells) that was significantly lower ($P < 0.001$; Student's t-test) than that measured in s-GO-treated networks (110 ± 6 s, n=18 cells, right plot in Figure 2 (b)). When $GABA_A$ receptors were pharmacologically blocked by bicuculline (20 μM; 20 min), an antagonist of inhibitory connections known to potentiate rhythmic activity patterns[23,26,27], the control IEI average value was still significantly lower ($P < 0.001$; Student's t-test) than that measured in s-GO neurons in the presence of the $GABA_A$ receptor antagonist (18 ± 1 s, n = 20 control cells, *vs* 92 ± 10 s, n = 18 s-GO cells; plot in Figure 2 (b), right). This indicated a direct reduction in the excitatory activity due to s-GO exposure.

Next we recorded single cell synaptic activity in the presence of TTX (1 μM, Figure 3 (a)). Under these experimental conditions synaptic currents, termed miniature PSCs (mPSCs), do not depend on action potential generation. mPSCs are due to the stochastic fusion of neurotransmitter vesicles at the presynaptic membrane and their frequency is proportional to the number of synaptic contacts[28]. Despite the fact that in the recorded hippocampal neurons spontaneous synaptic activity was manifested as inward currents (in our recording conditions, see Supporting Information[21]) made up by a mixed population of inhibitory ($GABA_A$receptor-mediated) and excitatory (AMPA glutamate receptor-mediated) PSCs, virtually all mPSCs, as previously reported[22], were identified as excitatory by their fast kinetics (decay time constant τ=

4 ± 0.3 ms, see Supporting Information[22]). Notably, s-GO significantly decreased ($P < 0.001$, Student's t-test; see plots in Figure 3 (a)) the frequency of mPSCs without affecting their amplitude (0.06 ± 0.02 Hz and 30 ± 0.7 pA, control, n = 15; 0.02 ± 0.001 Hz and 26 ± 0.7 pA, s-GO-treated n= 9; summarized in Figure 3 (a)). To ascertain whether the s-GO interference with synaptic activity was selective on glutamate-mediated fast synaptic transmission, we tested the occurrence of evoked inhibitory PSCs by pair recordings of mono-synaptically coupled neurons[22] (Supplementary Information and Figure S6a) and we observed that s-GO apparently did not impair $GABA_A$ mediated connections.

To determine whether changes in excitatory synaptic density may account for the reduction in fast- mPSC frequency detected in s-GO treated cultures, neurons were co-immunostained for β-tubulin III and the vesicular glutamate transporter (VGLUT1), a transmembrane protein localized at the glutamatergic presynaptic terminals[29]. Antibody to VGLUT1 labeled presynaptic boutons under both conditions (Figure 3b). Using β-tubulin III labeling to identify neuronal bodies and dendrites, we quantified VGLUT1-positive puncta, detecting a significant ($P < 0.001$; Student's t-test) reduction in their density in s-GO treated samples (control $1.4 \times 10^{-3} \pm 0.045 \times 10^{-3}$ n= 6 fields and s-GO $0.28 \times 10^{-3} \pm 0.11 \times 10^{-3}$ n= 6 fields, plot in Figure 3 (b)). Parallel experiments were performed to quantify GABAergic synapses, by similar co-staining but for the vesicular GABA transporter (VGAT) to localize presynaptic GABAergic terminals[22,30]. These studies indicated that s-GO incubation did not alter the inhibitory connection density (Supporting Information and Figure S6b).

Figure 3

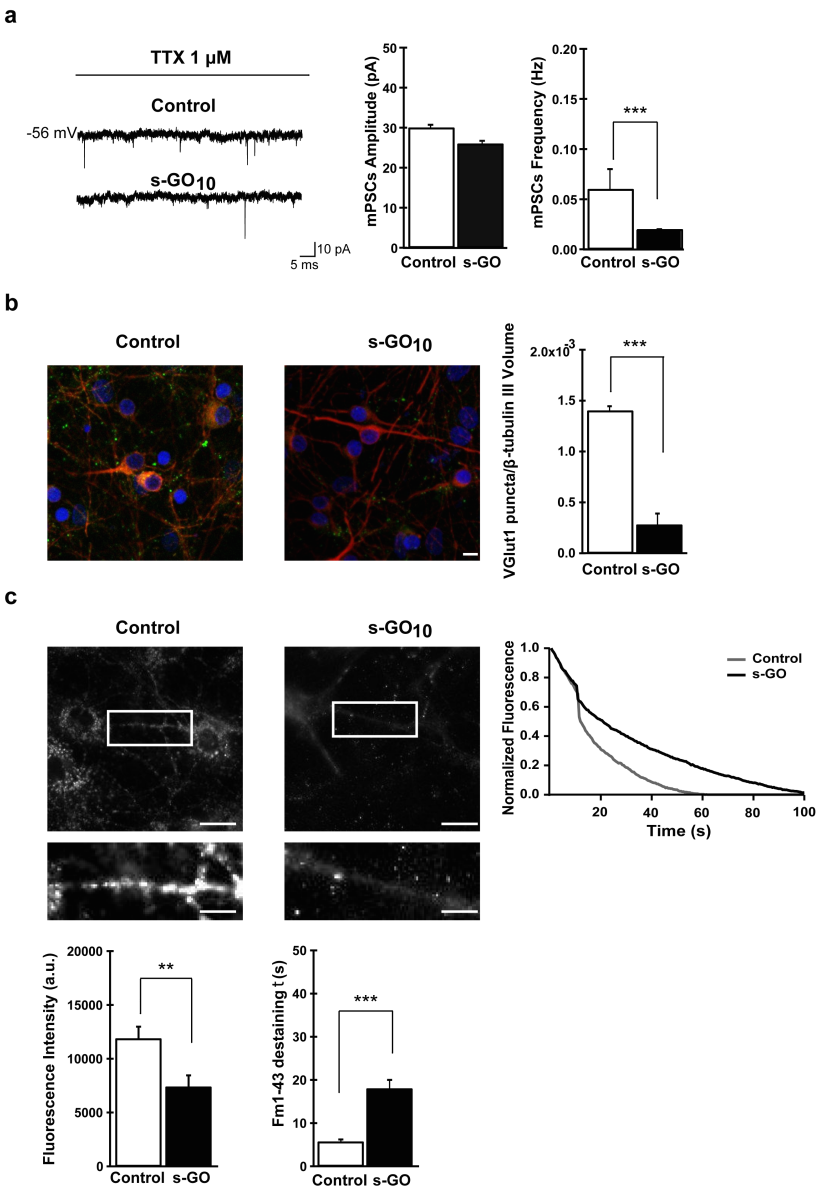

Figure 3. *s-GO exposure at high concentration impaired excitatory synapses.* In (a) sample tracings of mPSCs recorded in control and s-GO-treated cultures (left panel). Right panel: plots reporting mPSC amplitude and frequency values. s-GO-treatment significantly decreased the frequency of mPSCs (*** = $P < 0.001$ Student's-t-test). In (b) confocal reconstruction of control and s-GO treated neurons immunolabeled for the vesicular glutamate transporter 1 (VGLUT1; green) and counterstained for cytoskeletal component β-tubulin III (red; nuclei are visualized by DAPI in blue; scale bar 10 µm). The plot shows the significant decrease of VGLUT1-positive puncta in s-GO-treated cultures (*** = $P < 0.001$ Student's-t-test). In (c) top, fluorescence images following staining with FM1-43, control and s-GO-treated. Scale bar 50 µm. The areas in the boxes are higher magnifications to highlight the difference in vesicular staining between the two conditions (scale bar 100 µm). The plot (top right) reproduces the representative (control and s-GO) traces of FM1-43 de-staining (please note that each trace has been normalized to the maximum fluorescence detected). Bottom: the left plot summarizes the initial raw fluorescent intensities of hippocampal terminals from control and s-GO-treated cultures (** = $P < 0.01$ Mann-Whitney test); the right plot summarizes the decay time constant τ of FM1-43 de-staining in the two conditions (*** = $P < 0.001$, Mann-Whitney test).

In the next set of experiments we measured the kinetics of synaptic vesicle release by real-time imaging of vesicles labeled with FM dye to monitor the rate of presynaptic vesicle recycling from hippocampal neurons treated or untreated with s-GO. After staining with the lipophilic dye FM1-43[31-33] clusters of presynaptic terminals were visible as bright fluorescence spots (Figure 3 (c)). The fluorescence intensity measured on FM-positive puncta following high KCl (50 mM;[34]) depolarization is proportional to the number of vesicles endocytosed during synaptic vesicle recycling, and thus, allows to estimate the size of the recycling vesicle pool[34]. In s-GO treated cells, upon high-K^+-loading protocol, we detected a significant ($P < 0.01$; Mann-Whitney test) reduction in the raw fluorescence intensity of FM1-43-positive hippocampal terminals (control 11876 ± 1100 arbitrary units –a.u.-, n= 7 fields; s-GO-treated 7400 ± 1057 a.u., n= 6 fields; 3 different culture series; Figure 3 (c)), suggesting that chronic incubation with s-GO decreased the recycling vesicle pool. When analyzing the decay time constant (τ) of the FM1-43 fluorescence de-staining profiles during vesicle exocytosis, we observed a significant ($P < 0.001$; Mann-Whitney test) difference in the kinetics displayed by control (τ= 5.7 ± 0.5 s, n = 205 terminals) and s-GO (τ= 18 ± 2 s, n = 85 terminals) treated cells, as summarized in Figure 3 (c). In reference experiments, image series captured on FM1-43 stained cells but without the high-K^+ de-staining stimulus, produced a baseline reference plot (not shown). Taken together, these results support the specific ability of chronic exposure to s-GO flakes to reduce the amount of excitatory synaptic contacts and to interfere with presynaptic vesicle recycling.

To test the ability of s-GO to impair cell membrane dynamics in general, we investigated whether s-GO (10 μg/mL) was also reducing exocytosis and recycling of synaptic-like microvesicles (MVs[15]) from cultured primary glial cells (see Supplementary Information). MVs are released into the extracellular space by direct budding from the plasma membrane of astrocytes, and have been shown to contribute to intercellular communication[15,35,36]. We treated pure glial cell cultures with s-GO (10 μg/mL) for 6-8 days. In Figure 4 (a) immunofluorescence staining of control and s-GO treated GFAP-positive cells are shown. s-GO incubation did not affect astrocyte density (Figure 4 (a) right histograms; n= 20 fields for both conditions) excluding any cytotoxic effect. In glial cultures MVs release was induced by bzATP incubation (100μM, 30 min, n= 3 different series of cultures[37-39]), and MVs release was detected and quantified by immunoblot analysis of the collected supernatant. In control, bzATP stimulation induced the appearance of the band corresponding to flotillin-1 (Figure 4 (c), bottom blot), a signature of MVs release[40-42]. Surprisingly, in s-GO treated astrocytes, the bzATP stimulation induced a marked increase in the size of the flotillin-1 band. This band was also detected in the absence of stimulation (Figure 4 (c) bottom blot) suggesting that s-GO *per se* induced MVs constitutive release.

AFM micrographs, show in Figure 4 (b) (left panel) the presence of vesicles in the stimulated control supernatant appearing as circular spots protruding from the ultra-flat mica surface. For each of them, width and height were independently measured from particle crossing height profiles and the resulting distributions were plotted (Figure 4 (b) right panel). Intriguingly, similar experiments with GR (10 μg/mL) did not induce shedding of MVs in glial cell cultures (Supplementary Information and Figure S7).

We also attempted to investigate the effect of increased lateral size of GO (l-GO, with a lateral dimension in the few μm range; 10 μg/mL final concentration) on cultured hippocampal cells. However, after 6-8 days of incubation, we measured a significant ($P < 0.001$; Student's t-test; Figure 4 (d)) reduction in both neuron and glial cell densities (control 160 ± 10 neurons/mm^2 and 96 ± 10 astrocytes/mm^2; l-GO-treated 96 ± 10 neurons/mm^2 and 40 ± 7 astrocytes/mm^2; n=10 visual fields each, 3 series of cultures; Figure 4 (d)) indicating cell toxicity that prevented any further functional measurements. We believe further investigations are warranted to explore such lateral size-dependent cytotoxic responses.

Figure 4

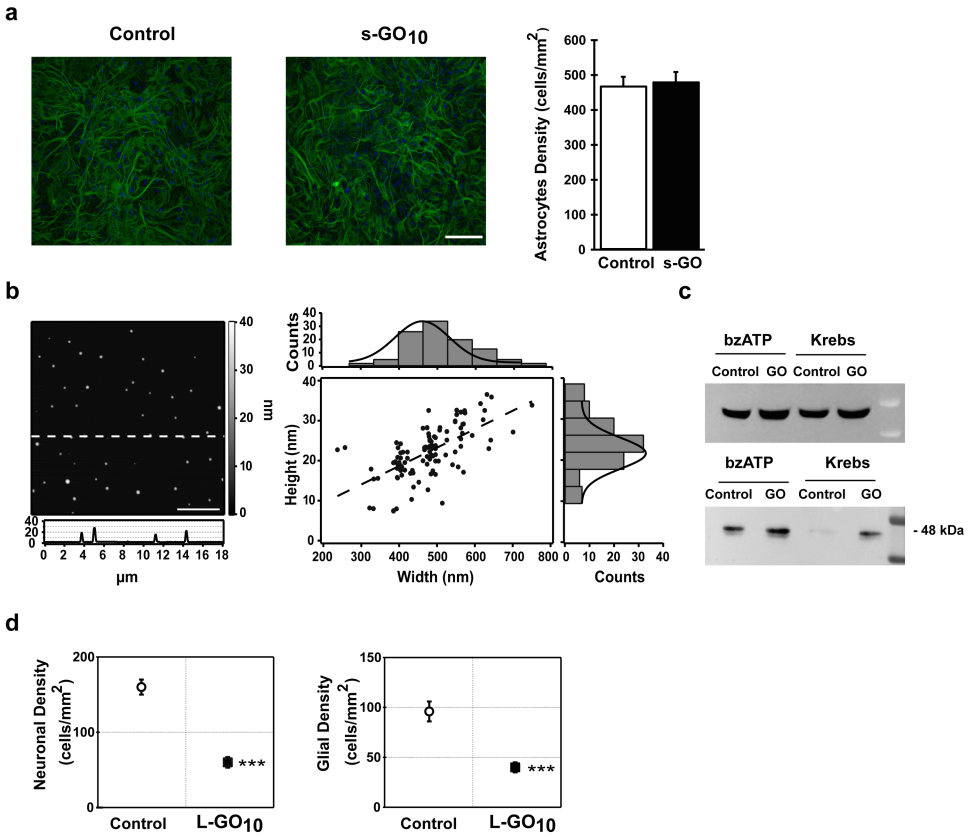

Figure 4. *s-GO exposure and microvesicles release in glial cells.* In (a) immunolabeling of primary rat astrocytes (3 weeks) in control and s-GO treated cells (10 µg/mL 6-8 days). Both cultures were immune-stained for GFAP (green) and nuclei visualized by DAPI (blue; scale bar: 100 µm). No statistical significance was found between the two conditions (top right). In (b) AFM image of fixed MVs where the differences in color are representative of height differences (brighter means higher). A representative height profile crossing 3 MVs is reported. The scatter plot (right) shows MVs width versus height distribution and is fitted with a regression line represented by the equation y = 0.046x + 0.218. A frequency histogram, built upon experimental measurements of both width and height, was plotted over each axis of the scatter graph, and fitted with Gaussian distributions. The frequency histograms revealed the highest number of occurrences to be about 490 nm and 24 nm for width and height, respectively. In (c) Western blotting of the pellets (bottom row) and cell lysates (top row) for the MVs marker flotillin-1. Pellets were obtained from the medium of glial cultures treated or un-treated with s-GO, under 2 different conditions: stimulated and not stimulated (Krebs) by 100 µM BzATP. Note the marked increase of the band for flotillin-1 in s-GO treated cells. In (d) plots summarizing the decreased density of hippocampal cells when treated with L-GO (~ 10 μm lateral size; 10 μg/mL final concentration).

We report here the ability of s-GO nanosheets to interfere specifically with neuronal synapses, without affecting cell viability. In particular, in cultured neuronal networks, upon chronic s-GO exposure, glutamatergic release sites were sized down. This was shown by: i) the reduction in frequency of spontaneous synaptic activity (PSCs and mPSCs) together with the marked reduction in VGLUT1-positive labeling[43], ii) the reduced probability of finding active neurons when network were explored by Ca^{++}-imaging[23,44] and iii) the decreased recycle vesicle pool quantified by FM1-43 measures together with the altered kinetic of vesicle recycling[34]. This down-regulation of glutamate-mediated synapses was apparently not due to a general cell-membrane disruption or to neuronal cell loss. In fact, we never detected alterations in basic electrophysiological parameters, reflecting neuronal health and membrane integrity[18-20].

In addition, cell densities in treated cultures were comparable to control ones. The survival of GFAP-positive glial cells was also not affected by s-GO exposure, both in mixed neuronal and in pure neuroglial cultures. In the latter condition, MVs release was indirectly monitored by the blot analysis of flotillin-1 protein[40,41], and MVs presence confirmed by direct AFM measures. In these cultures, exposure to s-GO stimulated the basal release of shed vesicles and augmented the bzATP-induced one[37-39]. s-GO increase in MVs release from neuroglia cells might be related to a general cell-stress condition[15] ultimately due to s-GO glial-membrane interactions or even internalization, depending on the flakes' shape, lateral dimension and oxidization degree[10] as well as the degree of protein adsorption from the culturing milieu[45].

Based on our experimental evidence we cannot rule out that treatment with s-GO down regulated the synaptic function (in particular presynaptic release) via MVs released in mixed neuronal-glial cultures, thus excluding a direct, membrane interference of s-GO nanosheets at the pre-synaptic glutamatergic terminals. MVs have long been reported as active messengers of intercellular communication, rather than mere inert debris[37], however, to our knowledge, there are no reports of astrocyte shed-MVs acting as regulators of synaptic activity. On the contrary, MVs released by microglia have been reported to affect synaptic activity, mainly acting at the presynaptic site of the excitatory synapses, but increasing synaptic activity and release in primary cultures[37]. Against this neuroglial-cell mediated response to s-GO is also the fact that astrocyte density in mixed cultures is artificially kept at a low level by the culturing procedure in itself, while the surviving microglia are even fewer[46].

In contrast to s-GO, the inert nature of GR flakes regarding synaptic activity and MVs release by glia is also of interest. This could be due to differences in shape and lateral size affecting flake-membrane interactions[10]. It is also interesting to consider that GR have a much less hydrophilic surface character and overall poorer dispersibility in cell culture media[45] that may lead to the formation of aggregates potentially unable to interact with sub-microscopic structures (such as the synaptic clefts).

The apparent selectivity in terms of the presynaptic terminals targeted by s-GO was also notable, with the inhibitory, GABAergic ones that remained unaffected, as evidenced by pair recordings and the VGAT labeling[22]. Given the ability of graphene flakes to undergo motion and vibration that can lead to interaction with and possible piercing of lipid bilayers[8], we propose an alternative mechanistic interpretation of our synaptic results. s-GO flakes may prevent the synaptic vesicle endocytotic cycle because their dimensions allow them to interact with the presynaptic cell membrane at the periphery of the synaptic cleft and then be up-taken by vesicles. In this process, the flakes may transiently trap vesicles in an open mode and prevent their closing and the subsequent endocytosis. This could affect synaptic release in the short term inducing, in the long term, a down regulation of glutamatergic release sites and synapses. To note, glutamatergic synaptic activity is specifically affected also when neurons are transiently exposed to s-GO, with a short-term up-regulation of release, turned into a down regulation within the first 3 days of chronic exposure (Figure S8 in Supplementary Information). The mechanism of such interaction among s-GO flakes and vesicles could be similar to what has been previously described for dispersed single walled carbon nanotubes[47]. In this context, the unlikeliness of affecting GABAergic terminals may reside in the different dimensions of the excitatory (16 nm) and inhibitory (10 nm) synaptic clefts[48]. The latter reported to be even narrowed to 6 nm at the periphery of the clefts due to transcleft elements while docked vesicles are concentrated at the central cleft domain[48]. On the contrary, docked vesicles in excitatory synapses are distributed evenly over the synaptic cleft[48]. It is tempting to speculate that these synaptic ultra-structural differences might explain why glutamatergic terminals became ideal targets to s-GO interactions. This selectivity is supported by the notion that, even when transiently exposed to s-GO via pressure ejected brief pulses, GABAergic synapses are unaffected (see Supplementary Information).

Regardless of the mechanisms involved, the ability of s-GO to alter synapses and induce glial cell reaction has not been previously documented. This might compromise neuronal signaling and CNS functions and seems crucially dependent on the GO sheet dimensions, since larger flakes were found unequivocally cytotoxic. In our experiments 6 days exposure of cultures to equal amounts of dispersed l-GO induced unequivocal hippocampal cell loss, both neuroglia and neurons, thus hampering any further evaluation of membrane/flakes interactions.
These observations deserve further studies, in fact, altering synapses and inducing glia reactivity may raise concerns from the safety and nanotoxicity point of view[49].

Beyond the safe design of nanomaterials, such a subtle interference affecting exquisite CNS signaling may offer possibilities in neuropharmacology, when specific targeting of excitatory synapses is desired[50-52]. The use of nanoparticles as therapeutics is in fact fueled by their ability to circumvent biological barriers[53] and targeting of synapses has created the basis for theranostics applications[54]. Our observations with thin s-GO flakes illustrate the potential of 2D nanosheet physical properties to engineer novel and specific glutamate-transmission modulators. It is also relevant to note that synapse formation and function in neuronal networks, when interfaced to planar graphene-based materials, are not affected[55]. This strengthens the notion that when exploring the application of graphene in biology, studies should be performed with well-characterized types of materials, since the materials' physical-chemical features, including geometry, are governing the potential interactions with specific biological components[2].

Methods

Materials and Methods are described in the Associated Content and Figures

ASSOCIATED CONTENT

Supporting Information: Materials and Methods, Supporting Results, Figure S1- S8 and Tables S1-S2.

AUTHOR INFORMATION

Corresponding Author

* Laura Ballerini International School for Advanced Studies (SISSA) via Bonomea 265 I-34136 Trieste phone +39 0403787779, LB laura.ballerini@sissa.it

Author Contributions

R.R. and A.F. performed cell biology, electrophysiology and immunofluorescence experiments and analysis; R.R. and F.P.U.S. design and performed imaging and real-time imaging experiments and analysis; N.L. and K.K. contributed to the synthesis and characterization of thin graphene oxide (l-GO and s-GO) of biological-grade; V.L. and E.V. contributed to the synthesis and characterization of pristine graphene (GR); M.M. performed glial cell experiments, immunofluorescence and western blot; D.S., I.R. and L.C. designed and performed the AFM experiments; L.B. and M.P. conceived the study; L.B. conceived the experimental design and contributed to the analysis of data; L.B. wrote the manuscript. All authors have given approval to the final version of the manuscript.

Funding Sources

We acknowledge financial support from the EU FP7-ICT-2013-FET-F GRAPHENE Flagship project (no. 604391), from the NEUROSCAFFOLDS-FP7-NMP-604263 and PRIN-MIUR n. 2012MYESZW.

Notes

The authors declare no competing financial interest.

ACKNOWLEDGMENTS

We are especially grateful to Micaela Grandolfo, Jessica Franzot and Beatrice Pastore for supervising the synaptic immune staining and quantification, the glial cell culturing and western blot experiments. IOM-TASC national laboratory (Trieste) is also gratefully acknowledged for AFM assistance. N.L. acknowledges Leon Newman for assistance with the TEM and Raman instrumentation. X-ray photoelectron spectra were performed at the National EPSRC XPS User's Service (NEXUS) at Newcastle University, an EPSRC Mid-Range Facility. N.L. acknowledges Mr. Leon Newman for assistance with the TEM and Raman instrumentation and Dr Nigel Hodson of the University of Manchester BioAFM Facility for his expert advice. The Antolin Group is also acknowledged for the provision of the commercial material. We acknowledge financial support from the EU FP7-ICT-2013-FET-F GRAPHENE Flagship project (no. 604391), from the NEUROSCAFFOLDS-FP7-NMP-604263 and PRIN-MIUR n. 2012MYESZW.

REFERENCES

1. Sanchez, V.C.; Jachak, A.; Hurt, R.H.; Kane, A.B. *Chem Res Toxicol.* **2012**, 25, 15-34.
2. Kostarelos, K; Novoselov, K.S. *Science* **2014**, 344, 261-263.
3. Mao, H.Y.; Laurent, S.; Chen, W.; Akhavan, O.; Imani, M.; Ashkarran, A.A.; Mahmoudi, M. *Chem Rev.* **2013**, 113, 3407-3424.

4. Bitounis, D.; Ali-Boucetta, H.; Hong, B.H.; Min, D.H.; Kostarelos, K. *Adv Mater.* **2013**, 25, 2258-2268.
5. Krishna, K.V.; Ménard-Moyon, C.; Verma, S.; Bianco, A. *Nanomedicine* (Lond) **2013**, 8, 1669-1688.
6. Wang, Y.; Li, Z.; Wang, J.; Li, J.; Lin, Y. *Trends Biotechnol.* **2011**, 29, 205-212.
7. Kuzum, D.; Takano, H.; Shim, E.; Reed, J.C.; Juul, H.; Richardson, A.G.; de Vries, J.; Bink, H.; Dichter, M.A.; Lucas, T.H.; Coulter, D.A.; Litt Li, B. *Nat Commun.* **2015**, 5, 5259-5263.
8. Li, Y.; Yuan, H.; von dem Bussche, A.; Creighton, M.; Hurt, R.H.; Kane, A.B.; Gao, H. *Proc Natl Acad Sci* U S A. **2013**, 110, 12295-12300.
9. Tu, Y.; Lv, M.; Xiu, P.; Huynh, T.; Zhang, M.; Castelli, M.; Liu, Z.; Huang, Q.; Fan, C.; Fang, H.; Zhou, R. *Nat Nanotechnol.* **2013**, 8, 594-601.
10. Mao, J.; Guo, R.; Yan, L. *Biomaterials* **2014**, 35, 6069-6077.
11. Rizzoli, S.O. *EMBO J.* **2014**, 33, 788-822.
12. Bianco, A. *Angew Chem Int Ed Engl.* **2013**, 52, 4986-4997.
13. Yang, D.; Li, T.; Xu, M.; Gao, F.; Yang, J.; Yang, Z.; Le, W. *Nanomedicine* (Lond) **2014**, 9, 2445-2455.
14. Zhang, Y.; Ali, S.F.; Dervishi, E.; Xu, Y.; Li, Z.; Casciano, D.; Biris, A.S. *ACS Nano* **2010**, 4, 3181-3186.
15. Falchi, A.M.; Sogos, V.; Saba, F.; Piras, M.; Congiu, T.; Piludu, M. *Histochem Cell Biol.* **2013**, 139, 221-231.
16. León, V.; Quintana, M.; Herrero, M.A.; Fierro, J.L.; de la Hoz, A.; Prato, M.; Vázquez, E. *ChemCommun* (Camb). **2011**, 47, 10936-10938
17. León, V.; Rodriguez, A.M.; Prieto, P.; Prato, M.; Vázquez, E. *ACS Nano* **2014**, 8, 563-571
18. Carp, J.S. *J Neurophysiol.* **1992**, 68, 1121-1132.
19. Gao, Y.; Liu, L.; Li, Q.; Wang, Y. *NeurosciLett.* **2015**, 591, 138-143.
20. Djuric, U.; Cheung, A.Y.; Zhang, W.; Mok, R.S.; Lai, W.; Piekna, A.; Hendry, J.A.; Ross, P.J.; Pasceri, P.; Kim, D.S.; Salter, M.W.; Ellis, J. *Neurobiol Dis.* **2015**, 76, 37-45.
21. Lovat, V.; Pantarotto, D.; Lagostena, L.; Cacciari, B.; Grandolfo, M.; Righi, M.; Spalluto, G.; Prato, M.; Ballerini, L. Nano Lett. **2005**, 5, 1107-1110.
22. Cellot, G.; Toma, F.M.; Varley, Z.K.; Laishram, J.; Villari, A.; Quintana, M.; Cipollone, S.; Prato, M.; Ballerini, L. J Neurosci. **2011**, 31, 12945-12953.
23. Bosi, S.; Rauti, R.; Laishram, J.; Turco, A.; Lonardoni, D.; Nieus, T.; Prato, M.; Scaini, D.; Ballerini, L. *Sci Rep.* **2015**, 5, 9562.
24. Stetter, O.; Battaglia, D.; Soriano, J.; Geisel, T. *PLoSComput Biol.* **2012**, 8.
25. Fabbro, A.; Pastore, B.; Nistri, A.; Ballerini, L. *Cell Calcium.* **2007**, 41, 317-329.

26. Tibau, E.; Valencia, M.; Soriano, J. *Front Neural Circuits* **2013**, 7, 199.
27. Sokal, D.M.; Mason, R.; Parker, T.L. *Neuropharmacology* **2000**, 39, 2408-2417.
28. Raastad, M.; Storm, J.F.; Andersen, P. *Eur J Neurosci.***1992**, 4, 113-117
29. Bellocchio, E.E.; Reimer, R.J.; Fremeau, R.T., Jr; Edwards, R.H. *Science* **2000**, 289, 870-876.
30. Moulder, K.L.; Jiang, X.; Taylor, A.A.; Shin, W.; Gillis, K.D.; Mennerick S. *J Neurosci.* **2007**, 27, 9846-9854.
31. Betz, W.J.; Bewick, G.S. *Science* **1982**, 255, 200-203
32. Ryan, T.A.; Reuter, H.; Wendland, B.; Schweizer, F.E.; Tsien, R.W.; Smith, S.J. *Neuron.* **1993**, 11, 713-724.
33. Betz, W.; Mao, F.; Smith, C. *Curr Opin Neurobiol.* **1996**, 6, 365-371.
34. Ryan, T.A. *Curr Opin Neurobiol.* **2001**, 11, 544-549.
35. Turola, E.; Furlan, R.; Bianco, F.; Matteoli, M.; Verderio, C. *Front Physiol.* **2012**, 3:149.
36. Frühbeis, C.; Fröhlich, D.; Kuo, W.P.; Krämer-Albers, E.M. *Front Cell Neurosci.* **2013**, 7, 182.
37. Antonucci, F.; Turola, E.; Riganti, L.; Caleo, M.; Gabrielli, M.; Perrotta, C.; Novellino, L.; Clementi, E.; Giussani, P.; Viani, P.; Matteoli, M.; Verderio, C. *EMBO J.* **2012**, 31, 1231-1240.
38. Bianco, F.; Pravettoni, E.; Colombo, A.; Schenk, U.; Möller, T.; Matteoli, M.; Verderio, C. *J Immunol.* **2005**, 174, 7268-7277.
39. Bianco, F.; Perrotta, C.; Novellino, L.; Francolini, M.; Riganti, L.; Menna, E.; Saglietti, L.; Schuchman, E.H.; Furlan, R; Clementi, E.; Matteoli, M.; Verderio C. *EMBO J.* **2009**, 28, 1043-1054
40. Del Conde, I.; Shrimpton, C.N.; Thiagarajan, P.; López, J.A. *Blood* **2005**, 106, 1604-1611.
41. Al-Nedawi, K.; Meehan, B.; Micallef, J.; Lhotak, V.; May, L.; Guha, A.; Rak, J.; *Nat Cell Biol.* **2008**, 10, 619-624.
42. Antonyak, M.A.; Cerione, R.A. *Methods Mol Biol.* **2014**, 1165,147-173.
43. Toyoshima, D.; Mandai, K.; Maruo, T.; Supriyanto, I.; Togashi, H.; Inoue, T.; Mori, M.; Takai, Y. *PLoS One.* **2014**, 27, 9-e89763.
44. Aguado, F.; Carmona, M.A.; Pozas, E.; Aguiló, A.; Martínez-Guijarro, F.J.; Alcantara, S.; Borrell, V.; Yuste, R.; Ibañez, C.F.; Soriano, E. *Development* **2003**, 130, 1267-1280.
45. Chong, Y.; Ge, C.; Yang, Z.; Garate, J.A.; Gu, Z.; Weber, J.K.; Liu, J.; Zhou, R. *ACS Nano.* **2015**, 9, 5713-5724.

46. Fabbro, A.; Sucapane, A.; Toma, F.M.; Calura, E.; Rizzetto, L.; Carrieri, C.; Roncaglia, P.; Martinelli, V.; Scaini, D.; Masten, L.; Turco, A.; Gustincich, S.; Prato, M.; Ballerini, L. *PLoS One*. **2013**, 8(8):e73621.
47. Malarkey, E.B.; Reyes, R.C.; Zhao, B.; Haddon, R.C.; Parpura, V. *Nano Lett*. **2008**, 8, 3538-3542.
48. High, B.; Cole, A.A.; Chen, X.; Reese, T.S. *Front Synaptic Neurosci*. **2015**, 7, 9.
49. Fedorovich, S.V.; Alekseenko, A.V.; Waseem, T.V. *Biochem Soc Trans.* **2010**, 38, 536-538.
50. Grados, M.A.; Atkins, E.B.; Kovacikova, G.I.; McVicar, E. *Psychology Res and Behavior Management PRBM* **2015**, 8, 115-131.
51. Gardoni, F.; Di Luca, M. *Curr Opin in Pharmacology* **2015** 20, 24-28.
52. Stone, J.M., *Ther Adv Psychopharmacol.* **2011**, 1, 5–18.
53. Meyer, R.A.; Sunshine, J.C.; Green, J.J. *Trends Biotechnol*. **2015**, 33, 514-524.
54. Borisova, T.; Nazarova, A.; Dekaliuk, M.; Krisanova, N.; Pozdnyakova, N.; Borysov, A.; Sivko, R.; Demchenko, A.P. *Int J Biochem Cell Biol*. **2015**, 59, 203-215.
55. Fabbro A.; Scaini D.; León V.; Vázquez E.; Cellot G.; Privitera G.; Lombardi L.; Torrisi F.; Tomarchio F.; Bonaccorso F.; Bosi S.; Ferrari A.C.; Ballerini L.; Prato M. *ACS Nano.* **2016**, 10, 615-23.